Acta Mech 234, 3979–4000 (2023)
https://doi.org/10.1007/s00707-023-03581-8

ORIGINAL PAPER

Mukul Saxena · Saikat Sarkar · J. N. Reddy

Modelling architected beam using a nonlocal derivative-free shear deformable beam theory

Received: 16 October 2022 / Revised: 6 March 2023 / Accepted: 20 April 2023 / Published online: 23 May 2023

Abstract It has been well established that the internal length scale related to the cell size plays a critical role in the response of architected structures. It this paper, a Volterra derivative-based approach for deriving nonlocal continuum laws directly from an energy expression without involving spatial derivatives of the displacement is proposed. A major aspect of the work is the introduction of a nonlocal derivative-free directionality term, which recovers the classical deformation gradient in the infinitesimal limit. The proposed directionality term avoids issues with correspondences under nonsymmetric conditions (such a unequal distribution of points that cause trouble with conventional correspondence-based approaches in peridynamics). Using this approach, we derive a nonlocal version of a shear deformable beam model in the form of integro-differential equations. As an application, buckling analysis of architected beams with different core shapes is performed. In this context, we also provide a physical basis for the consideration of energy for nonaffine (local bending) deformation. This removes the need for additional energy in an ad hoc manner towards suppressing zero-energy modes. The numerical results demonstrate that the proposed framework can accurately estimate the critical buckling load for a beam in comparison to 3-D simulations at a small fraction of the cost and computational time. Efficacy of the framework is demonstrated by analysing the responses of a deformable beam under different loads and boundary conditions.

1 Introduction

Architected materials (such as sandwich beams with periodic core unit cell) [1–3] have emerged as a light weight and low energy materials as alternatives to more traditional materials. The architected structures can potentially be used for applications across the length scales, from tissue engineering to the designing the body of an airport. Classical continuum mechanics (CCM) does not perform well in predicting the mechanical behaviour of these materials on a structural scale [4,5], since they involve complex internal geometry that contributes to the response. Therefore, a new challenge for the mechanicians is to address this by coming up with an appropriate model. One way would be to use the nonlocal continuum models [6]. The earliest such theory was proposed by the Cosserat brothers in the form of a generalized continuum theory, in which the material points in a solid body is assumed to have rotational degrees of freedom (dof) in addition to the usual translational dof [7]. Building on this concept, much later Eringen worked on different nonlocal continuum models, accounting for the nonlocal effects in the form of higher-order derivatives [8]. This was followed by a series of works on nonlocal theories [9,10] with many of its variants like couple-stress theory [11] and modified

M. Saxena · S. Sarkar (✉)
Department of Civil Engineering, Indian Institute of Technology Indore, Indore 453552, Madhya Pradesh, India
E-mail: saikat@iiti.ac.in

J. N. Reddy
Department of Mechanical Engineering, Texas A&M University, College Station, Tx 77845, United States

couple-stress theory [12–14]. However, certain nonlocal models may at times show anomalous results (e.g. anomalous stiffening effect). Moreover, some of these theories require higher-order derivative information that are difficult to be handled within a finite element (FE)-based formulation due to the requirements for high-order interelement continuity. Derivative-based evolution equations, in general, are inefficient in capturing sharp changes in the field variables like shock wave and discontinuities like crack. As a solution to these issues, a derivative-free theory named as peridynamics (PD) was introduced by Silling in 2000 [15–17]. The PD-based framework introduced the governing equations by directly invoking action at a distance rather than contact forces. These equations remain well posed even in the case of discontinuities [18–20]. However, the PD-based framework too has certain limitations; for example, the bond-based PD (BBPD) limits its applicability by constraining the Poisson's ratio. The BBPD fails to distinguish between the volumetric and distortional deformations. The state-based PD (ordinary and non-ordinary) overcomes such limitations by relaxing the restrictions on the bond forces. However, it is often difficult to arrive at strictly PD-based constitutive models.

One way to bypass these challenges is to have the "constitutive correspondence" between the PD and the classical continuum mechanics by defining a PD-based deformation gradient. But such extension may suffer from instability issues originating from zero-energy mode-induced oscillations [21]. To avoid this, additional energy is typically introduced in the form of spring stiffness. However, such additional energy can change the solution completely and the correct amount is difficult to be estimated a priori. For many applications, detailed three-dimensional simulations are not feasible, and reduced dimensional models like beam, plate, and shell come out to be useful. These models have actually made CCM popular to a great extent. For nonlocal theories also, focus has been on nonlocalizing these reduced dimensional models; one may refer to [9,10] and [22–24] for bending and buckling analysis of nonlocal beams and plates, respectively.

In this work, we introduce a nonlocal derivative-free continuum theory (DFCT), in which the governing equations are arrived at in the form of integro-differential equations, from an energy expression using Volterra derivative. Specifically, we derive a nonlocal version of the Timoshenko shear deformable beam model without involving spatial derivatives. A crucial aspect of our theory is the derivation of a derivative-free deformation gradient, which recovers the classical deformation gradient in the infinitesimal limit. Another important aspect of the work is to consider the energy corresponding to the local nonaffine deformation of the beam. This provides a physical basis for adding extra energy in an ad hoc manner for suppressing the zero-energy modes. Overall, the approach presented here has the following advantages:

(1) We propose a novel way of computing deformation map that does not suffer from the problems of the commonly used gradient term, when particle distribution is nonuniform.
(2) We derive the governing equations in the form of integro-differential equations using Volterra derivative from a total energy functional that accounts for nonaffine deformation of the beam. This is crucial to eliminate the zero-energy modes that afflict the PD solution without adding extra energy on an ad hoc basis.
(3) Such formulation is particularly important for capturing the deformation of architected materials where individual members undergo localized deformation, which is difficult to be captured in the traditional way. We demonstrate the efficacy of this approach by modelling a micro-architected beam and comparing with full three-dimensional solutions as well as solutions based on micropolar beams. In each case, the approach outlined here provides a better solution.

While the theory can be seen as a variant of the PD, we call the present theory as the DFCT. Here, the directionality term differs from its PD counterpart due to a bias correction operation, which plays a crucial role when there is a loss of symmetry. The efficacy of the framework is demonstrated by analysing the responses of a shear deformable beam under different loading and boundary conditions.

The rest of the paper is organized as follows. In Sect. 2, a Volterra derivative-based approach is adopted to propose the derivative-free governing equations for the shear deformable beam. The mainstay of the paper is the proposal of a directionality term, which approaches its classical counterpart in the infinitesimal limit. In Sect. 3, the nonlocal derivative-free governing equations for buckling of shear deformable beam are proposed to compute the required additional energy. This section showcases the efficacy of the proposed formalism in precisely estimating the critical buckling load of the shear deformable beam. This section also suggests a meaningful way of imposing different boundary conditions. The numerical implementation of the derive-free model is discussed in Sect. 4, where the additional energy obtained through buckling analysis is adopted to capture the transverse deformations in the prismatic and non-prismatic (corrugated) shear deformable beams. The efficacy of the proposed formalism has been showcased by examining the beam under different loading and boundary conditions. To demonstrate the efficacy of proposed formalism, we further examine the sandwich

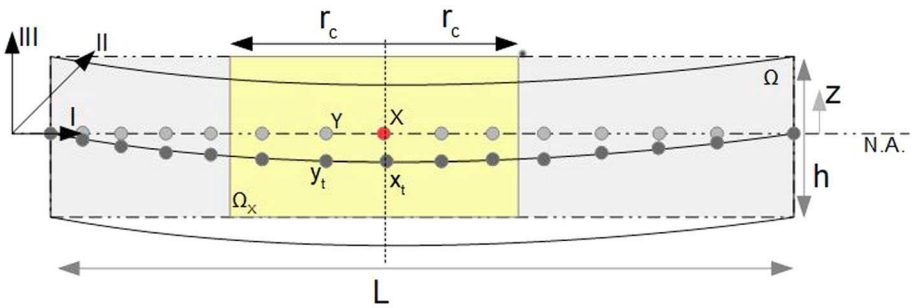

Fig. 1 Pictorial representation of a shear deformable beam presenting the undeformed beam in dashed lines and deformed configuration of beam using solid lines. The dots in the yellow region represent the neighbourhood Y for a material point X

beam with periodic cores of different shapes and compare the response with different established theories. Finally, some concluding remarks are made in Sect. 5.

2 Mathematical formulation

The derivative-free continuum formalism bifurcates from the classical theory with the incorporation of a derivative-free deformation gradient. Presently, we discuss the theory in the context of deriving a derivative-free nonlocal version of the classical shear deformable beam model. Let us consider a beam of length L placed along the axis I as shown in Fig. 1, which experiences a transverse loading along the III-axis. The beam is assumed to have uniform width b, depth h and cross-sectional area $A = bh$. As per our formalism, a material point X is assumed to interact nonlocally within an influence domain Ω_X of finite influence radius r_c. The volume of the influence domain of the material point X is represented by V_X, which is computed upon discretization as, V_X=$2r_chb$. As shown in Figure 1, x_t and y_t denote the deformed positions at time t of their respective undeformed material points X and Y. The deformed and undeformed location of neutral axis is denoted by $(N.A.)_t$ and $(N.A.)_0$, respectively. The associated undeformed and deformed fibre lengths and the fibre stretch are expressed as $r_{XY} := Y - X$, $r_{xy} := y_t - x_t$ and $u_{XY} := r_{xy} - r_{XY}$, respectively.

2.1 Derivation of a nonlocal derivative-free directionality term

We would first derive a functional form for a derivative-free nonlocal directionality term, $\hat{G}(\xi, X)$, which is used to relate an undeformed fibre with the associated stretch, u_{XY} such that,

$$u_{XY} = \hat{G}(u, X) r_{XY}. \tag{1}$$

To avoid bias in the estimate of the directionality term, we first remove the drift information from Eq. (1). This step is crucial for a symmetry loss, as would be seen later in this paper:

$$u_{XY} - \bar{u}_X = \hat{G}(u, X)(r_{XY} - \bar{r}_X), \tag{2}$$

where

$$\begin{aligned} \bar{r}_X &= \frac{1}{V_X} \int_{\Omega_X} r_{XY} dY \\ \bar{u}_X &= \frac{1}{V_X} \int_{\Omega_X} u_{XY} dY. \end{aligned} \tag{3}$$

From here, we can get an expression for $\hat{G}$ indicated as follows:

$$\begin{aligned} &(u_{XY} - \bar{u}_X)(r_{XY} - \bar{r}_X)^T = \hat{G}(u, X)(r_{XY} - \bar{r}_X)(r_{XY} - \bar{r}_X)^T \\ &\implies \int_{\Omega_X} (u_{XY} - \bar{u}_X)(r_{XY} - \bar{r}_X)^T dY = \hat{G}(u, X) \int_{\Omega_X} (r_{XY} - \bar{r}_X)(r_{XY} - \bar{r}_X)^T dY \end{aligned}$$

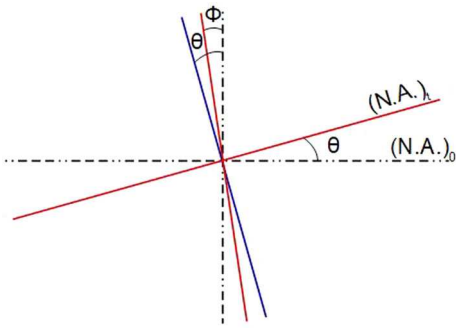

Fig. 2 Pictorial representation of shear deformation at any cross section in the shear deformable beam

$$\implies \hat{G}(u, X) = \left[\int_{\Omega_X} (u_{XY} - \bar{u}_X)(r_{XY} - \bar{r}_X)^T dY\right]\left[\int_{\Omega_X} (r_{XY} - \bar{r}_X)(r_{XY} - \bar{r}_X)^T dY\right]^{-1}. \quad (4)$$

From Eq. (4), it can be seen that $\hat{G}$ imparts the nonlocal attribute by considering the far-off interactions. One can also show that the derivative-free directionality term approaches its classical gradient counterpart in an infinitesimal limit (see Appendix A). It may be interesting to note that a similar expression for the directionality term was arrived at in the context of optimization, particle filtering and upscaling using a sophisticated stochastic projection technique [25–28]. We believe our present simple derivation at the continuum level would be useful and accessible to a larger audience.

2.2 Formulation of nonlocal derivative-free governing equations for a shear deformable beam

Consider that $u_X := \{(u_1)_X, (u_2)_X, (u_3)_X\}$ represents the displacement at a material point X along I, II and III axes, respectively, defined over the domain Ω (see Fig. 1). Since the shear deformable beam captures the deformation due to the coupled effect of shear and bending, the rotation θ about plane normal to the neutral axis in the deformed configuration may be related to the transverse displacement u_3 and shear deformation Φ through the equation as follows (see Fig. 2):

$$\theta_X = \hat{G}(u_3, X) - \Phi_X. \quad (5)$$

Recalling the inextensibility assumption of the shear deformable beam, the displacement field at the material point X, located at a distance z along the III-axis from the neutral axis, may be characterized as ([9,29]):

$$\begin{aligned} (u_1)_X &\approx (u_1^0)_X - z(\Phi)_X \\ (u_2)_X &= 0 \\ (u_3)_X &= (u_3^0)_X, \end{aligned} \quad (6)$$

where u_1^0 and u_3^0 represent the axial and lateral displacements, respectively, of the point at the neutral axis and Φ the rotation about the plane normal to the neutral axis in the deformed configuration. Using Eq. (6), the velocity $v := \{v_1, v_2, v_3\}$ at any material point in the beam takes the form:

$$\begin{aligned} (v_1)_X &= (\dot{u}_1)_X = -z(\dot{\Phi})_X \\ (v_2)_X &= (\dot{u}_2)_X = 0 \\ (v_3)_X &= (\dot{u}_3)_X. \end{aligned} \quad (7)$$

The Hamiltonian $\mathcal{H}$ for the beam can be written as the summation of the total kinetic energy, K, and the total potential energy, Ψ, of the system given as follows:

$$\mathcal{H} = K + \Psi. \quad (8)$$

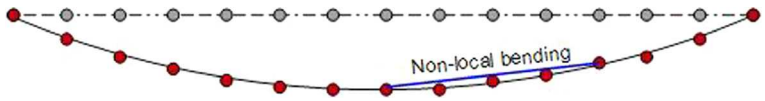

Fig. 3 Pictorial representation of nonlocal bending in the shear deformable beam

Let p denote the momentum at a material point and ρ the mass density. The kinetic energy term (K) may be expressed in the continuum limit as ([30]):

$$\begin{aligned} K &= \int_\Omega \frac{p\cdot p}{2\rho} d\Omega \\ \implies K &= \int_\Omega \frac{1}{2}\rho\left((\dot{u}_1^2)_X + (\dot{u}_3^2)_X\right) d\Omega \\ \implies K &= \int_0^L \int_{-h/2}^{h/2} \frac{b}{2}\rho\left((\dot{u}_1^2)_X + (\dot{u}_3^2)_X\right) dz dX \\ \implies K &= \int_0^L \int_{-h/2}^{h/2} \frac{b}{2}\rho\left(z^2(\dot{\Phi}^2)_X + (\dot{u}_3^2)_X\right) dz dX \\ \implies K &= \int_0^L \frac{1}{2}\rho\left(I(\dot{\Phi}^2)_X + A(\dot{u}_3^2)_X\right) dX, \end{aligned} \tag{9}$$

where $I = \int_{-h/2}^{h/2} bz^2 dz$ represents the second moment of area and $A = \int_{-h/2}^{h/2} b dz$ is the area of the cross section. The total potential energy (Ψ) for the nonaffine deformation of the beam can be expressed as the summation of the potential energy due to axial stretching (Ψ_A), shear deformation (Ψ_S), nonlocal bending deformation (Ψ_{NLB}) and work done by externally applied transverse load q acting per unit length of the beam (Ψ_q), that is,

$$\Psi = \Psi_A + \Psi_S + \Psi_{NLB} - \Psi_q. \tag{10}$$

$$\begin{aligned} \Psi =& \int_0^L \frac{1}{2} EA\left(\hat{G}(u_1, X)\right)^2 dX + \int_0^L \frac{1}{2} k_s \beta A\left(\hat{G}(u_3, X) - \Phi\right)^2 dX \\ &+ \frac{1}{2V_X}\int_0^L \int_{\Omega_X} \gamma \frac{EI}{L^2}\left((u_3)_Y - (u_3)_X\right)^2 dY dX - \int_0^L \frac{1}{2} q u_3^2 dX, \end{aligned} \tag{11}$$

where E denotes the Young's modulus of elasticity and β denotes the shear modulus of elasticity. The third term on the right-hand side of the above equation accounts for the nonaffine deformation arising from the nonlocal bending between the two material points (see Fig. 3) and is assumed that

$$\text{Nonlocal bending stiffness} \propto \frac{EI}{L^2}.$$

Accordingly, $\gamma \frac{EI}{L^2}$ (with γ being a proportionality constant) denotes the nonlocal interparticle bending stiffness along the direction of u_3. We shall shortly see that the third energy term vanishes in the infinitesimal limit (i.e. with vanishing nonlocality). Using Eq. (2),

$$(u_3)_Y - (u_3)_X = \hat{G}(u_3, X) r_{XY}. \tag{12}$$

Equation (11) takes the following form:

$$\begin{aligned} \Psi =& \int_0^L \frac{1}{2} EA\left(\hat{G}(u_1, X)\right)^2 dX + \int_0^L \frac{1}{2} k_s \beta A\left(\hat{G}(u_3, X) - \Phi\right)^2 dX \\ &+ \frac{1}{2}\int_0^L \frac{1}{V_X}\int_{\Omega_X} \gamma \frac{EI}{L^2}\left(\hat{G}(u_3, X) r_{XY}\right)^2 dY dX - \int_0^L \frac{1}{2} q u_3^2 dX \\ \implies \Psi =& \int_0^L \frac{1}{2} EA\left(\hat{G}(u_1, X)\right)^2 dX + \int_0^L \frac{1}{2} k_s \beta A\left(\hat{G}(u_3, X) - \Phi\right)^2 dX \end{aligned} \tag{13}$$

$$
\begin{aligned}
&+\frac{1}{4r_c}\int_0^L \gamma\frac{EI}{L^2}\left(\hat{G}(u_3,X)\right)^2\int_{\Omega_X}(r_{XY})^2\,dYdX-\int_0^L\frac{1}{2}qu_3^2dX\\
\implies \Psi&=\int_0^L\frac{1}{2}EA\left(\hat{G}(u_1,X)\right)^2dX+\int_0^L\frac{1}{2}k_s\beta A\left(\hat{G}(u_3,X)-\Phi\right)^2dX\\
&+\frac{r_c^3}{6r_c}\int_0^L\gamma\frac{EI}{L^2}\left(\hat{G}(u_3,X)\right)^2dX-\int_0^L\frac{1}{2}qu_3^2dX\\
\implies \Psi&=\int_0^L\frac{1}{2}EA\left(\hat{G}(u_1,X)\right)^2dX+\int_0^L\frac{1}{2}k_s\beta A\left(\hat{G}(u_3,X)-\Phi\right)^2dX\\
&+\frac{1}{2}\int_0^L\vartheta\left(\hat{G}(u_3,X)\right)^2dX-\int_0^L\frac{1}{2}qu_3^2dX,
\end{aligned}
\tag{14}
$$

where $\vartheta=\frac{\gamma EIr_c^2}{3L^2}$, from which we can see that $\vartheta\to 0$ as the nonlocality diminishes ($r_c\to 0$) recovering the classical energy expression for the shear deformable beam. A pictorial representation of the same is presented in Fig. 3. Using Eq. (6), the above equation may further be written as:

$$
\begin{aligned}
\Psi&=\int_0^L\frac{1}{2}EA\left(\hat{G}(z\Phi,X)\right)^2dX+\int_0^L\frac{1}{2}k_s\beta A\left(\hat{G}(u_3,X)-\Phi\right)^2dX\\
&+\int_0^L\frac{1}{2}\vartheta\left(\hat{G}(u_3,X)\right)^2dX-\int_0^L\frac{1}{2}qu_3^2dX\\
\implies \Psi&=\int_0^L\frac{1}{2}Eb\int_{-h/2}^{h/2}dz\left(\hat{G}(z\Phi,X)\right)^2dX+\int_0^L\frac{1}{2}k_s\beta A\left(\hat{G}(u_3,X)-\Phi\right)^2dX\\
&+\int_0^L\frac{1}{2}\vartheta\left(\hat{G}(u_3,X)\right)^2dX-\int_0^L\frac{1}{2}qu_3^2dX\\
\implies \Psi&=\int_0^L\frac{1}{2}EI\left(\hat{G}(\Phi,X)\right)^2dX+\int_0^L\frac{1}{2}k_s\beta A\left(\hat{G}(u_3,X)-\Phi\right)^2dX\\
&+\int_0^L\frac{1}{2}\vartheta\left(\hat{G}(u_3,X)\right)^2dX-\int_0^L\frac{1}{2}qu_3^2dX.
\end{aligned}
\tag{15}
$$

Using Volterra derivative as discussed in ([6]), the equations of motion of an elastodynamic continuum are given by

$$
\begin{aligned}
\dot{p}&=-\frac{\delta\mathcal{H}}{\delta u}=-\frac{\delta\Psi}{\delta u}\\
&\implies \dot{p}(\Phi)=-\frac{\delta\Psi}{\delta\Phi}\quad and\quad \dot{p}(u_3)=-\frac{\delta\Psi}{\delta u_3}.
\end{aligned}
\tag{16}
$$

The first nonlocal derivative-free governing equations for Timoshenko beam may be obtained by

$$
\dot{p}(\Phi)=-\frac{\delta\mathcal{H}}{\delta\Phi}.
\tag{17}
$$

From Eq. (16), it can be computed that

$$
\begin{aligned}
&\dot{p}(\Phi)=\rho I\ddot{\Phi}\\
&\frac{\delta\Psi}{\delta\Phi}=\frac{\delta}{\delta\Phi}\left[\int_0^L\frac{1}{2}EI\left(\hat{G}\left(\Phi,X\right)\right)^2dX+\int_0^L\frac{1}{2}k_s\beta A\left(\hat{G}\left(u_3,X\right)-\Phi\right)^2dX\right]\\
&\implies \frac{\delta\Psi}{\delta\Phi}=-\hat{G}\left(EI\delta\hat{G}(\Phi,X),X\right)-k_s\beta A\left(\hat{G}\left(u_3,X\right)-\Phi\right)\\
&\implies \rho I\ddot{\phi}=EI\hat{G}\left(\hat{G}\left(\Phi,X\right),X\right)+k_s\beta A\left(\hat{G}(u_3,X)-\Phi\right).
\end{aligned}
\tag{18}
$$

Similarly, the second governing equation may be computedas:

$$
\begin{aligned}
&\dot{p}(u_3) = -\frac{\delta H}{\delta u_3} \\
&\dot{p}(u_3) = \rho A \ddot{u}_3 \\
&\frac{\delta \Psi}{\delta u_3} = \frac{\delta}{\delta u_3}\left[\int_0^L \frac{1}{2} k_s \beta A \left(\hat{G}(u_3, X) - \Phi\right)^2 + \int_0^L \frac{1}{2}\vartheta \left(\hat{G}\left(u_3, X\right)\right)^2 - \int_0^L \frac{1}{2} q u_3^2 dX\right] \\
&\quad \Longrightarrow \frac{\delta \Psi}{\delta u_3} = -\left(\hat{G}\left(k_s \beta A \hat{G}(u_3, X), X\right) - \hat{G}(\phi, X)\right) - \vartheta \hat{G}\left(\hat{G}(u_3, X), X\right) - q \\
&\quad \Longrightarrow \rho A \ddot{u}_3 = k_s \beta A \left(\hat{G}\left(\hat{G}(u_3, X), X\right) - \hat{G}(\phi, X)\right) + \vartheta \hat{G}\left(\hat{G}(u_3, X), X\right) + q. \qquad (19)
\end{aligned}
$$

Therefore, the nonlocal derivative-free governing equations may be written as

$$
\begin{aligned}
&\rho I \ddot{\phi} = E I \hat{G}\left(\hat{G}\left(\Phi, X\right), X\right) + k_s \beta A \left(\hat{G}(u_3, X) - \Phi\right) \\
&\rho A \ddot{u}_3 = k_s \beta A \left(\hat{G}\left(\hat{G}(u_3, X), X\right) - \hat{G}(\phi, X)\right) + \vartheta \hat{G}\left(\hat{G}(u_3, X), X\right) + q.
\end{aligned} \qquad (20)
$$

3 Buckling analysis of shear deformable beam

Similarly, the nonlocal derivative-free counterparts of the governing equations for the buckling analysis of the shear deformable beam, subjected to axial compressive load P, may be written as

$$
\begin{aligned}
&E I \hat{G}\left(\hat{G}\left(\Phi, X\right), X\right) + k_s \beta A \left(\hat{G}\left(u_3, X\right) - \Phi\right) = 0 \\
&k_s \beta A \left(\hat{G}\left(\hat{G}\left(u_3, X\right), X\right) - \hat{G}\left(\Phi, X\right)\right) - P \hat{G}\left(\hat{G}\left(u_3, X\right), X\right) + \vartheta \hat{G}\left(\hat{G}\left(u_3, X\right), X\right) = 0. \qquad (21)
\end{aligned}
$$

The above equations can be decoupled as

$$
\begin{aligned}
&\hat{G}(\hat{G}(\hat{G}(\Phi, X), X), X) + \Lambda \hat{G}(\Phi, X) = 0 \\
&\hat{G}(\hat{G}(\hat{G}(\hat{G}(u_3, X), X), X), X) + \Lambda \hat{G}(\hat{G}(u_3, X), X) = 0,
\end{aligned} \qquad (22)
$$

where

$$
\Lambda = \frac{(P - \vartheta)/(EI)}{\left(\frac{P-\vartheta}{k_s \beta A}\right) - 1}. \qquad (23)
$$

The general solution for the nonlocal decoupled equations for buckling analysis can be written as

$$
\begin{aligned}
u_3 &= C_1 \cos\sqrt{\Lambda} X + C_2 \sin\sqrt{\Lambda} X + C_3 X + C_4 \\
\Phi &= C_5 \sin\sqrt{\Lambda} X + C_6 \sqrt{\Lambda}\eta \cos\sqrt{\Lambda} X + C_7.
\end{aligned} \qquad (24)
$$

Given that the general solution for the nonlocal equations must satisfy the governing equations, substituting Eq. (24) in Eq. (22) and comparing the coefficient of each term, we arrive at

$$
\begin{aligned}
u_3 &= C_1 \cos\sqrt{\Lambda} X + C_2 \sin\sqrt{\Lambda} X + C_3 X + C_4 \\
\Phi &= -C_2 \sqrt{\Lambda}\eta \cos\sqrt{\Lambda} X + C_1 \sqrt{\Lambda}\eta \sin\sqrt{\Lambda} X - C_3,
\end{aligned} \qquad (25)
$$

where η is a constant parameter and $\{C_1, C_2, C_3, C_4\}$ are constants that can be obtained using the boundary conditions. For the first case, we begin with simply supported end conditions, i.e. $u_3 = 0$ and $E I \hat{G}(\Phi, X) = 0$ at $x = 0$ and $x = L$:

$$
\begin{aligned}
&\hat{G}(\Phi, X) = \frac{-12\eta}{r_c^3 \sqrt{\Lambda}}\left(r_c \sqrt{\Lambda} \cos\left(\frac{r_c\sqrt{\Lambda}}{2}\right) - 2\sin\left(\frac{r_c\sqrt{\Lambda}}{2}\right)\right)\left(C_1 \cos\left(\sqrt{\Lambda} X\right) + C_2 \sin\left(\sqrt{\Lambda} X\right)\right) \\
&\hat{G}(\Phi, X) = \zeta\left(C_1 \cos\left(\sqrt{\Lambda} X\right) + C_2 \sin\left(\sqrt{\Lambda} X\right)\right)
\end{aligned}
$$

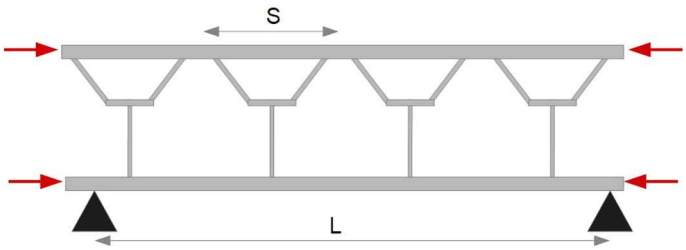

Fig. 4 Pictorial representation of the corrugated Timoshenko beam with Y-shaped core

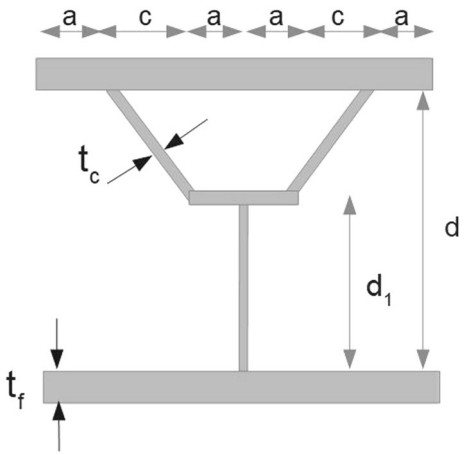

Fig. 5 Pictorial representation of the cross section of Y-shaped core of the corrugated Timoshenko beam

$$\zeta = \frac{-12\eta}{r_c^3\sqrt{\Lambda}}\left(r_c\sqrt{\Lambda}\cos\left(\frac{r_c\sqrt{\Lambda}}{2}\right) - 2\sin\left(\frac{r_c\sqrt{\Lambda}}{2}\right)\right). \tag{26}$$

Imposing the boundary conditions, we get

$$\begin{bmatrix} 1 & 0 & 0 & 1 \\ \cos\sqrt{\Lambda}L & \sin\sqrt{\Lambda}L & L & 1 \\ \zeta & 0 & 0 & 0 \\ \zeta\cos\sqrt{\Lambda}L & \zeta\sin\sqrt{\Lambda}L & 0 & 0 \end{bmatrix} \begin{Bmatrix} C_1 \\ C_2 \\ C_3 \\ C_4 \end{Bmatrix} = 0 \implies [A]\{C\} = 0. \tag{27}$$

For a nontrivial solution to exist, $|\ A\ |$ should vanish,

$$\sin\sqrt{\Lambda}L = 0 \tag{28}$$

$$\implies P_{cr} = \frac{\pi^2 EI\left(1 - \frac{\vartheta}{k_s\beta A}\right) - \vartheta L^2}{L^2 + \frac{\pi^2 EI}{k_s\beta A}}. \tag{29}$$

To perform the numerical analysis, we first take an example of a Y-shaped core beam. However, other core shapes have been examined in the later section. Using Eq. (29), we compute the critical load P_{cr} for a simply supported shear deformable beam with Y-shaped core. Figure 4 presents the pictorial representation of the Y-shaped core beam. Figure 5 presents the cross section of the Y-shaped core ([31]) with dimensions, $a = 0.002$ m, $s = 0.026$ m, $t_c = 0.0003$ m, $t_f = 0.001$ m, $d = 0.022$ m and $d_1 = 0.013$ m.

The value of s/L ratio is varied from 0.035 to 0.25, and the value of critical buckling load is computed using detailed 3-D Finite Element (FE) analysis. The first buckling mode is shown in Fig. 6. The obtained buckling load is used to compute the additional stiffness through Eq. (29).

Fig. 6 First buckling mode for sandwich beam with Y-shaped core obtained using 3-D FE analysis

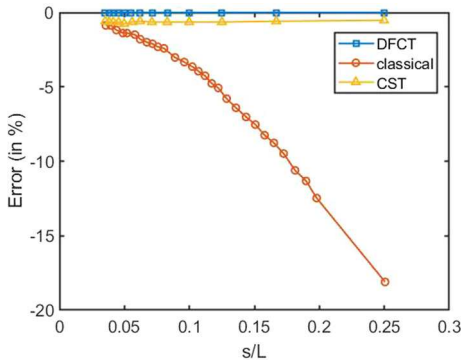

Fig. 7 Comparison of the relative percentage error obtained via different methodologies

Now, we define an error measure for comparing the performance of different methods, in which the 3-D FE results serve as a benchmark. The error is computed using the following formula:

$$Error = \frac{(P_{cr})_{method} - (P_{cr})_{3DFEM}}{(P_{cr})_{3DFEM}} \times 100. \tag{30}$$

The error % is computed for DFCT (with $\gamma = 2719.577$ for this particular example), classical theory ([31]), couple-stress theory (CST) ([31]) and is presented in Fig. 7. As can be seen from Fig. 7, the proposed framework can provide an accurate estimate of the critical buckling load.

3.1 Imposition of boundary condition (BC)-s using pseudo-nodes

One important aspect for the simulation of the integro-differential equations is the imposition of the boundary conditions. Therefore, before performing the deformation studies we address this by incorporating pseudo-nodes on each side of the beam. A fictitious region of length twice the influence radius is assumed on each boundary as shown in Figs. 8 and 9. Within a discretized set up, the BCs are given as follows:

Clamped BC:

$$\begin{aligned} &(i)\ \ (u_3)_{-\mathcal{P}} = (u_3)_{\mathcal{P}} \\ &(ii)\ \ \Phi_{-\mathcal{P}} = -\Phi_{\mathcal{P}}, \end{aligned} \tag{31}$$

where $\mathcal{P} = 1, 2, 3, \ldots$ denote the discretization nodes and $\mathcal{P} = -1, -2, -3, \ldots$ denote the node on the extended boundary.

Simply supported BC:

$$\begin{aligned} &(i)\ \ (u_3)_{-\mathcal{P}} = -(u_3)_{\mathcal{P}} \\ &(ii)\ \ \Phi_{-\mathcal{P}} = \Phi_{\mathcal{P}} \quad \text{where } \mathcal{P} = 1, 2, 3, ... \\ &(iii)\ \ \hat{G}(\hat{G}(u_3, X), X) = \hat{G}(\Phi, X). \end{aligned} \tag{32}$$

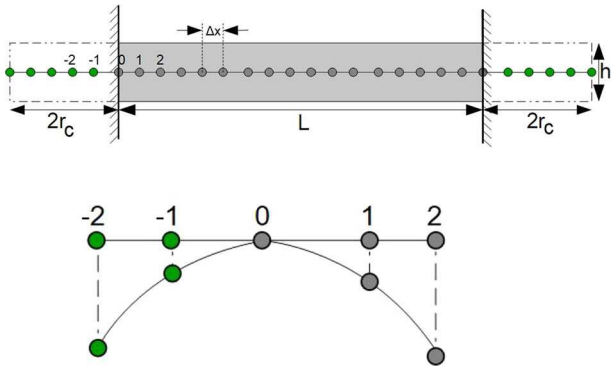

Fig. 8 Boundary effect minimization for a clamped boundary condition

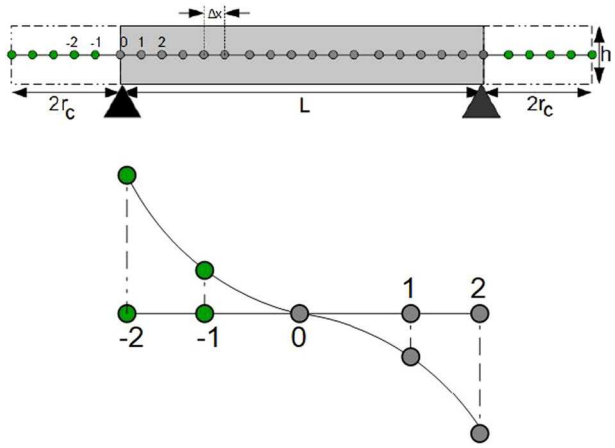

Fig. 9 Boundary effect minimization for a simply support boundary condition

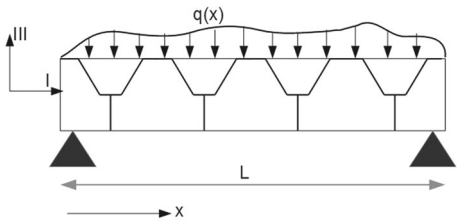

Fig. 10 Pictorial representation of the shear deformable beam with Y-shaped core subjected to transverse loading

4 Numerical results

4.1 Analysis of shear deformable beam with Y-shaped core

For numerical simulation, we begin with the analysis of a corrugated shear deformable beam subjected to transverse load. A pictorial representation of the beam is presented in Fig. 10. For studying the shear deformable beam, the derivative-free nonlocal equations are simulated in the strong form.

The undeformed length of the beam is considered as $L = 0.6477m$. The cross-sectional area A and second moment of area I are assumed to be the same as given in the previous section. The mechanical properties of the beam, i.e. Young's modulus $E = 209GPa$ and the mass density $\rho = 7850\,kg/m^3$, are considered with the time step taken as $\Delta t = 1\mu s$. To investigate the importance of the additional term in effectively capturing the nonlocal bending effect, we first examine the response of the simply supported beam when subjected to uniformly distributed load $q(x) = 1000N/m$. The simply supported BCs are implemented through Eq. (32). Figure 11 presents the importance of additional nonlocal bending energy in arriving at a stabilized solution.

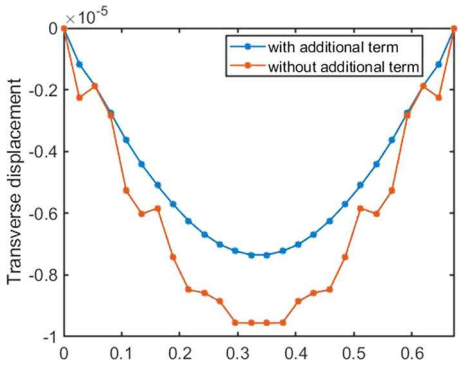

Fig. 11 The effect of additional term in stabilizing the nonlocal solution obtained via DFCT

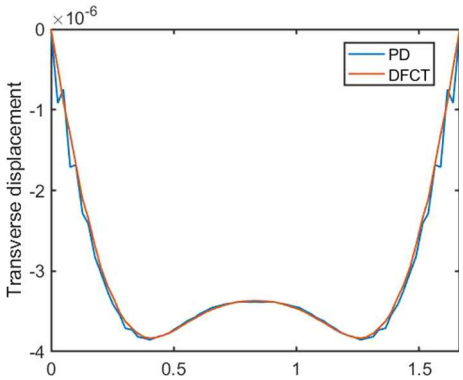

Fig. 12 Comparison of results obtained via PD and DFCT, after incorporating the additional term

To demonstrate the advantages of the proposed formalism over a PD correspondence, in the context of loss of symmetry, a random discretization of nodes is considered. The undeformed length of the beam is taken as $L = 1.667m$. The pseudo-boundaries are implemented through Eq. (32). The dynamic analysis is performed using a time step $\Delta t = 3\mu s$. The responses obtained via the PD and the DFCT are recorded and presented in Fig. 12 (at time $t_f = 1500\mu s$). The DFCT-based response presents the stabilized solution for the energy obtained through buckling analysis performed in the previous section. However, the zero-energy mode oscillations still persist in PD analysis Fig. 13 and Fig. 14.

We further extend our study to demonstrate the efficacy of DFCT in obtaining the stabilized solution under the application of unsymmetrical transverse loading. For this purpose, we analyse the response of the corrugated beam when subjected to a uniformly varying load (UVL) $q(x) = q_0\left(1 - \frac{x}{L}\right)$ and a parabolic loading $q(x) = q_0\left(1 - \frac{x}{L}\right)^2$, where $q_0 = 1000N/m$. The responses for the UVL and parabolic loading are presented in Fig. 13 and Fig. 14. Figure 14 demonstrates the efficacy of the DFCT over PD in suppressing the zero-energy oscillations with the nonlocal bending energy.

4.2 Analysis of a prismatic shear deformable beam

To examine the accuracy of the proposed formalism in determining the response of a prismatic shear deformable beam, we consider a steel beam of length $L = 1.538m$, cross-sectional area $A = 7196.8 \times 10^{-6}m^2$ and second moment of area $I = 2.01 \times 10^{-5}m^4$. The Young's modulus of elasticity and mass density of the material is considered as $E = 210GPa$ and $\rho = 7850\,kg/m^3$, respectively. The experimental value of buckling load $P_{cr} = 3779kN$ for the column of same dimension has been suggested by [32]. This value of P_{cr} is substituted in Eq. (29) to compute the coefficient $\gamma = 1.88 \times 10^6$, which is further incorporated to analyse the response of the beam when subjected to uniformly distributed load $q_0 = 1000N/m$. The simply supported boundary conditions are incorporated through Eq. (32). The transverse and rotational displacement for a randomly discretized beam (with mean interparticle spacing $\Delta X = 0.0034m$) is presented in Fig. 15 and Fig. 16. The

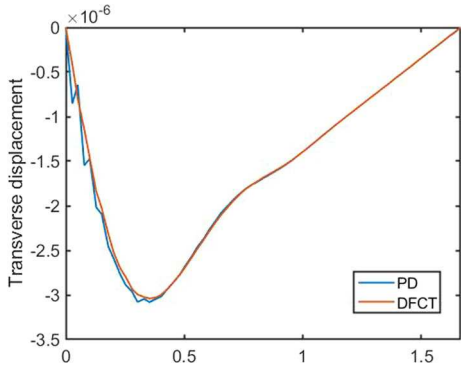

Fig. 13 Comparison of the response recorded via PD and DFCT for simply supported shear deformable beam with Y-shaped core when subjected to uniformly distributed load

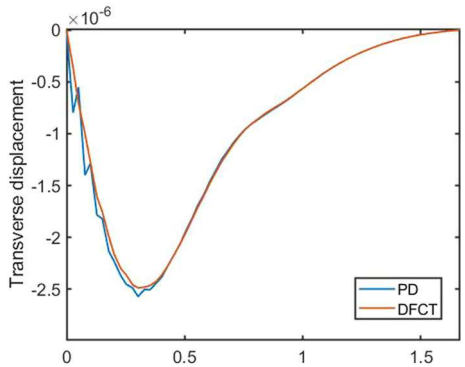

Fig. 14 Comparison of the response recorded via PD and DFCT for simply supported shear deformable beam with Y-shaped core when subjected to parabolic loading

DFCT-based response presents the stabilized solution for the energy obtained through buckling analysis. However, the zero-energy mode oscillations still persist in PD analysis.

Since concrete is one of the most widely used construction material, we further extend our study to examine the response of concrete beams. For the numerical simulations, a prismatic beam of length $L = 10m$ is considered with the depth, h, and the width, b, of beam taken as $2\,m$ and $1\,m$, respectively. For the numerical analysis, we consider $M40$ grade of concrete (with $\rho = 2400\,kg/m^3$, $\mu = 0.3$ and $E = 5000\sqrt{f_{ck}}MPa$, where f_{ck} denotes the characteristic compressive strength of a particular grade of concrete). A shear correction factor $k_s = 5/6$ is used. A time step of $1\mu s$ is chosen for analysing the dynamic response of the beam under varying loading and boundary conditions. The shear deformable beam subjected to varying external loading is randomly discretized using 450 particles. The radius of influence is taken as $r_c = 46.2mm$.

4.2.1 A clamped–clamped beam subjected to a uniformly distributed loading

The beam is clamped at both the ends. The boundary conditions in terms of u_3 and Φ are imposed using Eq. (31). The beam is analysed for $t_f = 500\mu s$. We begin with the analysis of the beam subjected to uniformly distributed load of intensity $q_0 = 1000N/m$.

The curves presented in Fig. 18a to Fig. 17 show the responses via DFCT and PD. A portion of Fig. 18a (marked with dotted rectangle) is zoomed in and is presented in Fig. 18b to figure 17. for clear visualization of oscillations in PD, which are considerably reduced in the response captured via DFCT. A similar trend is observed in the rotational displacement, which is presented in Fig. 18.

4.2.2 A clamped–clamped beam subjected to a uniformly varying load

We further extend our study to analyse the response of the beam when subjected to a uniformly varying load as shown in Fig. 19

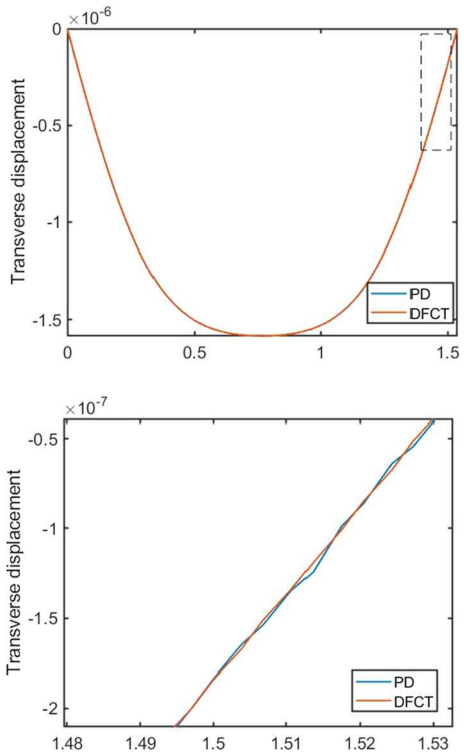

Fig. 15 Comparing the deformations in a simply supported beam subjected to uniformly distributed load. **a** Transverse deformation. **b** A zoomed view of transverse deformation: oscillations are observed in PD

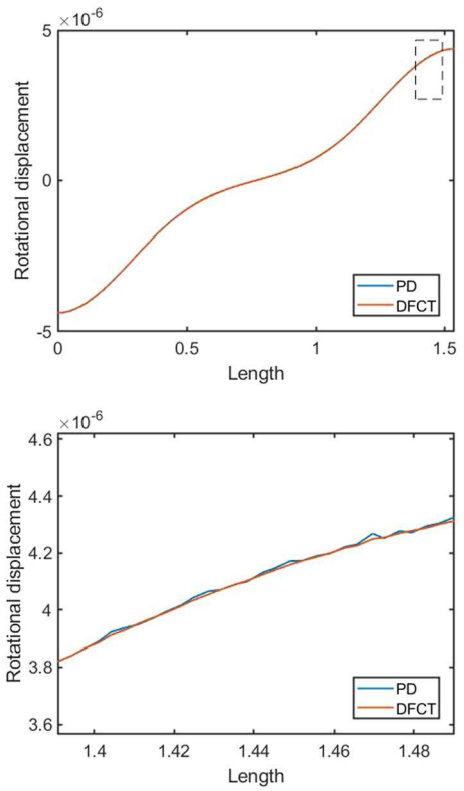

Fig. 16 Comparing the deformations in a simply supported beam subjected to uniformly distributed load. **a** Rotational displacement. **b** A zoomed view of rotational deformation: oscillations are observed in PD

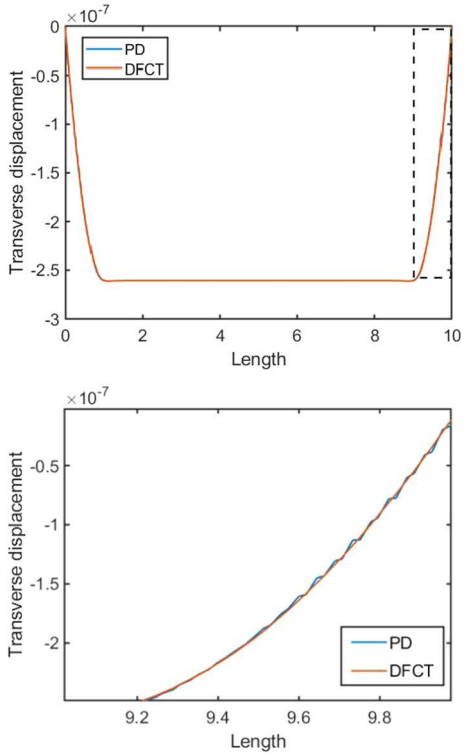

Fig. 17 Comparing the deformations in a clamped–clamped beam subjected to uniformly distributed load. **a** Transverse deformation. **b** A zoomed view of transverse deformation: oscillations are observed in PD

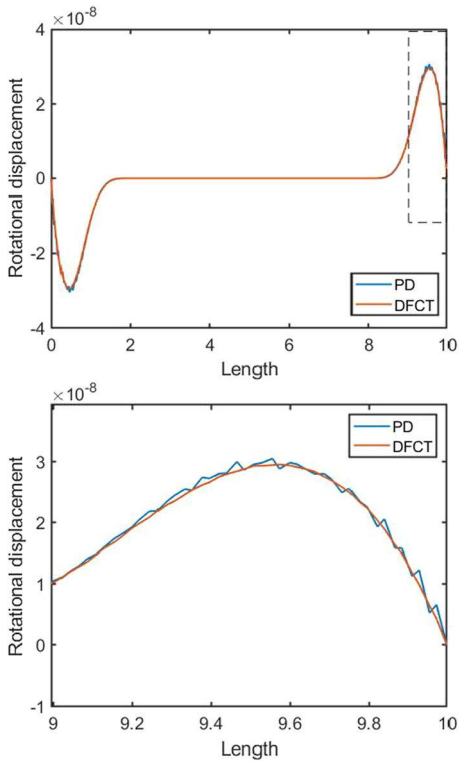

Fig. 18 Comparing the deformations in a clamped–clamped beam subjected to uniformly distributed load. **a** Rotational displacement. **b** A zoomed view of rotational deformation: oscillations are observed in PD

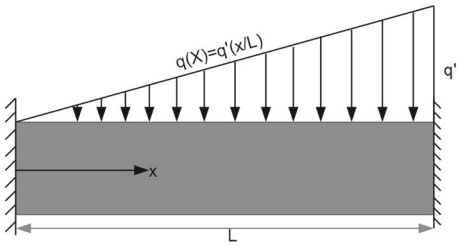

Fig. 19 Pictorial representation of a clamped–clamped beam subjected to a uniformly varying load

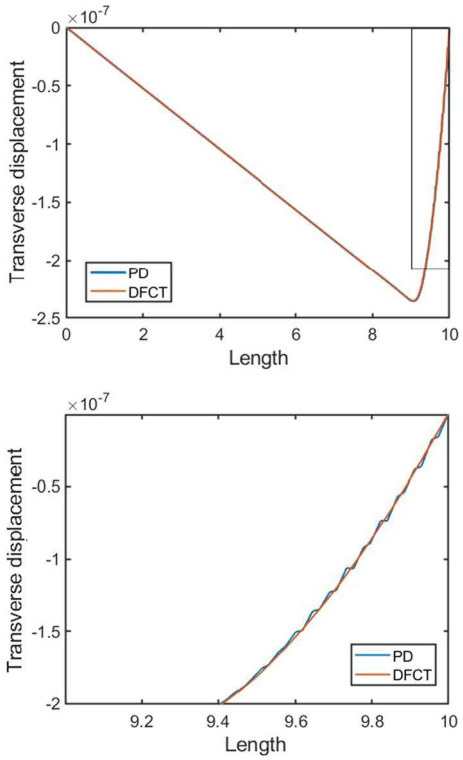

Fig. 20 Comparison between the response captured via PD and DFCT when the beam is subjected to a uniformly varying load. **a** Transverse displacement of the beam. **b** A zoomed view of transverse deformation: oscillations are observed in PD

The load intensity $q_0 = 1000N/m$ is applied, and the response is captured via PD and DFCT. Fig. 20 and Fig. 21 demonstrates the efficacy of proposed formalism in effectively minimizing the oscillations observed in the beam when subjected to unsymmetrical loading.

The curves presented in Fig. 20a report the oscillations in the transverse displacement response captured via PD. A portion of Fig. 20a, marked with dotted rectangle, is zoomed in for clear visualization of oscillations in PD, which are not seen in the response captured via DFCT (see Fig. 21b). Figure 21 shows the comparison of the rotational response obtained via two methodologies. The results are found in conformity as higher oscillations are observed in the case of PD as compared to DFCT.

4.3 A clamped–clamped beam subjected to parabolic loading

In our next example, we analyse the beam subjected to parabolic external loading. The load q at a distance x from the left support of the beam of length L may be defined as $q(x) = q_0 \left(\frac{x}{L}\right)^2$. The load intensity $q_0 = 1000N/m$. The response at $t_f = 500\mu s$ is presented in Fig. 22 and Fig. 23 to manifest the efficacy of proposed formalism in capturing the response of a shear deformable beam subjected to an unsymmetrical external loading.

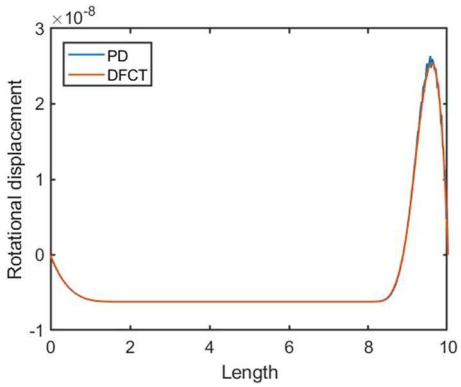

Fig. 21 Comparison between the rotational displacement captured via PD and DFCT when the beam is subjected to a uniformly varying load

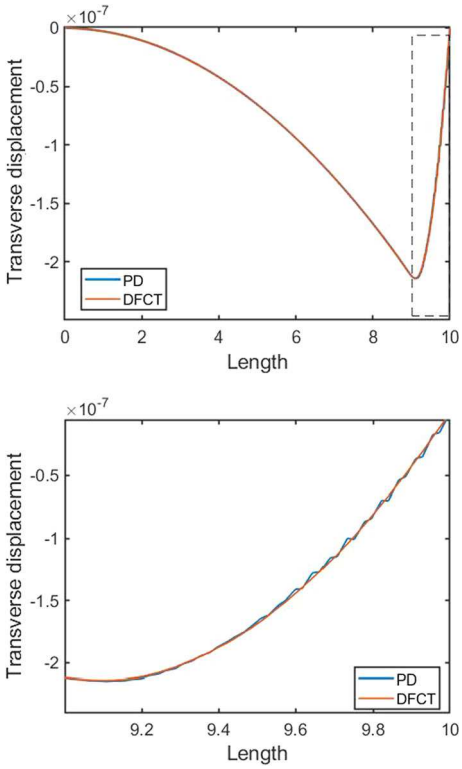

Fig. 22 Comparison between the response captured via PD and DFCT. **a** Transverse displacement of the beam. **b** A zoomed view of transverse deformation: oscillations are observed in PD

The transverse response of the beam subjected to parabolic loading is recorded and presented in Fig. 22a. Figure 22b magnifies the portion of Fig. 22a, enclosed by the rectangle with dotted lines, for a better visualization of oscillating response captured via PD. Figure 23 shows the comparison of the rotational response obtained via PD and DFCT.

4.3.1 A simply supported beam subjected to uniformly distributed loading

To demonstrate the efficacy under different boundary condition, we now examine the same shear deformable beam under simply supported boundary condition. The beam is subjected to a uniformly distributed external load of intensity $q_0 = 1000N/m$. A pictorial representation of the same is presented in Fig. 24.

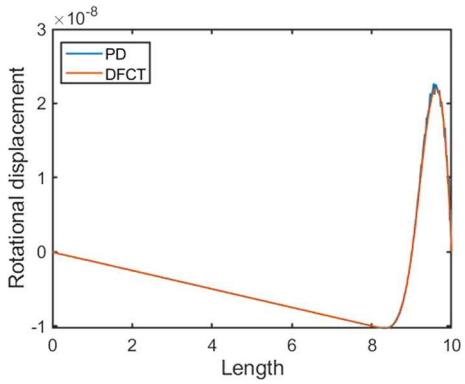

Fig. 23 Comparison between the rotational displacement captured via PD and DFCT

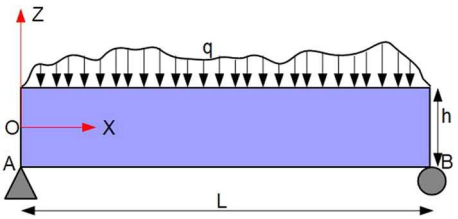

Fig. 24 Pictorial representation of a simply supported shear deformable beam subjected to uniformly distributed load throughout the span

The simply supported boundary conditions are imposed using Eq. (32). The response obtained at $t_f = 200\mu s$ is presented in Fig. 25 and Fig. 26. The transverse response of the simply supported shear deformable beam subjected to uniformly distributed load is presented in Fig. 25a. Figure 25b presents a magnified portion of 25a, enclosed by the rectangle with dotted lines, for a better visualization of oscillating response captured via PD. Figure 26a presents the rotational response obtained via PD and DFCT, and the zoomed section is presented in Fig. 26b. The figures demonstrate the presence of higher oscillations in the response obtained via PD. Therefore, it can be manifested that the proposed formalism, i.e. DFCT, is a better alternative for capturing the response of a shear deformable beam.

4.4 A simply supported sandwich beam with periodic core shapes subjected to three-point bending

To demonstrate the efficacy of the proposed formalism in precisely capturing the response of a simply supported shear deformable beam, we examine the sandwich beams with two different core shapes, i.e. web-core ($\alpha = 90°$) and truss-core ($\alpha = 60°$). In the first case, we study the response of a 2-m-long sandwich beam with web-core length $s = 0.2m$ and depth $d = 0.1m$ (as shown in Fig. 27a). The thickness of the core is taken as $0.005m$. For numerical analysis, we consider Young's modulus as $206GPa$ and Poisson's ratio as 0.3.

The buckling analysis of the web-core beam is performed using 3-D FE model as illustrated in Fig. 27b, c. The buckling load (P_{cr}) is recorded and presented in Table 1. The additional stiffness is then computed through Eq. (29). To demonstrate the efficacy of the proposed formalism, the beam is examined under three-point bending (as shown in Fig. 29a), and the results are then compared with the corresponding response obtained via 3-D FE, sandwich theory [31] and couple-stress theory (CST) [31]. The 3-D FE results serve as the benchmark for comparison with different methodologies and the relative error % by using Equation (30). Table 1 presents the comparison and error% ($\bar{E}$) for web-core sandwich beam with different cross-sectional properties.

For the next case, we consider a sandwich beam with truss-core unit cell ($\alpha = 60°$) which is repeated periodically along the length of the beam (as shown in Fig. 28b). The thickness of core is taken as $t_f = 0.005m$. The mechanical properties of the beam are same as in the case of web-core sandwich beam. Figure 28c represents the buckling response of the beam under simply supported boundary conditions.

The critical buckling load obtained from the buckling analysis is recorded and used to compute the extra stiffness term. The beam is further examined under three-point bending (as shown in Figure 29b), and the

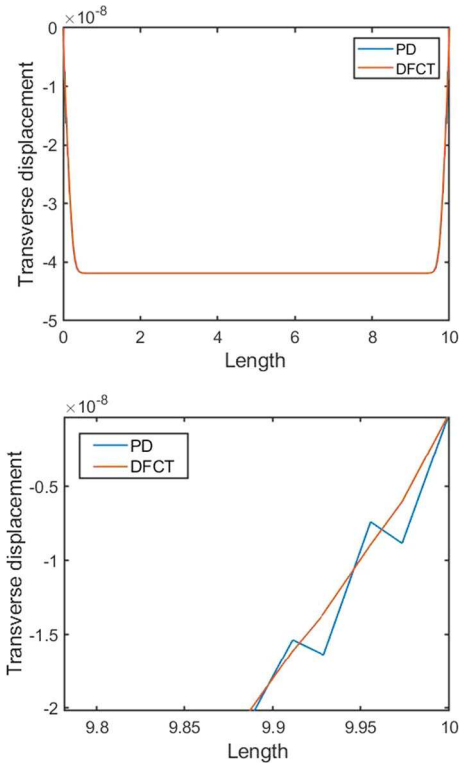

Fig. 25 Comparison between the transverse and rotational displacements obtained via PD and DFCT. **a** Transverse deflections. **b** A zoomed view of transverse deformation: oscillations are observed in PD

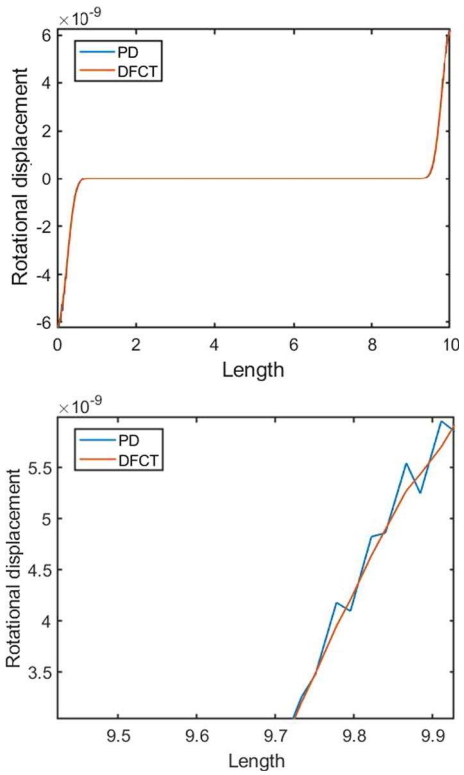

Fig. 26 Comparison between the transverse and rotational displacements obtained via PD and DFCT. **a** Rotational deflections. **b**A zoomed view of transverse deformation: oscillations are observed in PD

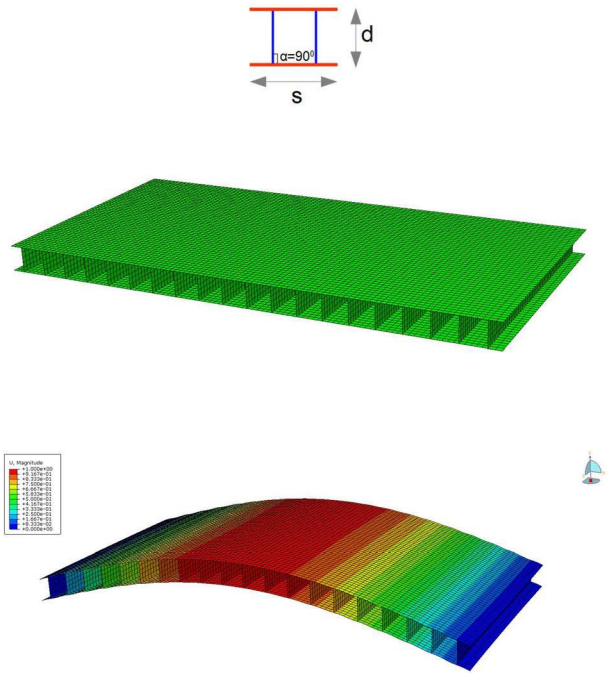

Fig. 27 **a** Unit cell of a web-core. **b** A schematic view of undeformed (meshed) web-core sandwich beam modelled using a 3-D FE software. **c** First buckling mode for a web-core sandwich beam using 3-D FE analysis

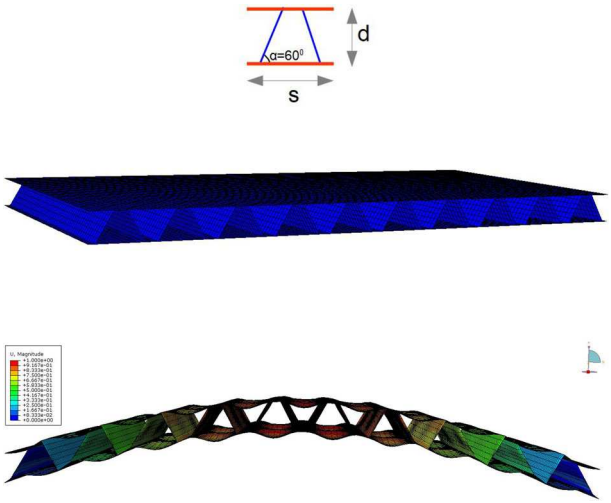

Fig. 28 **a** Unit cell of a truss-core. **b** A schematic view of undeformed (meshed) truss-core sandwich beam modelled using a 3-D FE software. **c** First buckling mode for a truss-core sandwich beam using 3-D FE analysis

result is validated through 3-D FE model. The result is recorded and further compared with those obtained via sandwich theory and CST (which are taken from [31]). Table 1 presents the comparison of maximum transverse deflection of the beam obtained via different methodologies.

It is interesting to note that the proposed formalism accurately captures the response for different core shapes and flange to core thickness ratio.

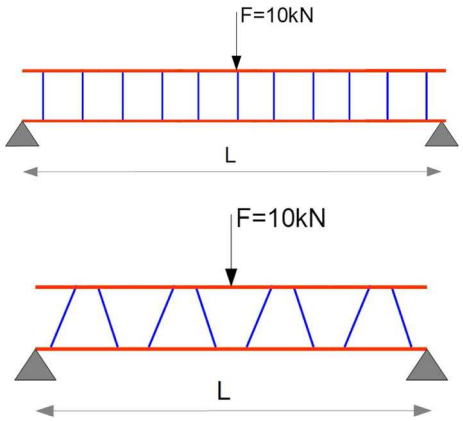

Fig. 29 A pictorial representation of simply supported shear deformable sandwich beam with **a** web-core and **b** truss-core unit cell subjected to three-point bending ($F = 10kN$)

Table 1 Maximum transverse deflection in a sandwich beam, predicted with present and validation models for $L = 2.0m$ beams subjected to three-point bending ($F = 10kN$)

S.no.	Periodic core shape	t_f/t_c	P_{cr} (in N)	Max. transverse deflection (in mm)			
				3D - FE	Sandwich theory ($\bar{E}$)	CST ($\bar{E}$)	DFCT ($\bar{E}$)
1.	Web-core ($\alpha = 90°$)	2	1.66×10^7	1.804	1.791 (-0.73%)	1.791 (-0.73%)	1.798 (-0.32%)
2.	Web-core ($\alpha = 90°$)	1	2.0797×10^6	2.843	2.810 (-1.17%)	2.810 (-1.17%)	2.815 (-0.98%)
3.	Truss-core ($\alpha = 60°$)	1	7.256×10^6	0.714	0.721 (0.98%)	0.718 (0.6%)	0.7155 (0.168%)

5 Conclusion

In this paper, we have introduced a Volterra derivative-based approach to derive the nonlocal continuum models without involving spatial derivatives. Specifically, we have derived the nonlocal integro-differential governing equations for a thick or shear deformable beam. The equations have been derived from a nonaffine energy of the beam, which plays a crucial role in addressing problems with the zero-energy modes that afflict the PD solutions without the addition of extra energy in an ad hoc manner. Another major aspect of the work has been the proposal of a derivative-free directionality term, which approaches its classical counterpart in the infinitesimal limit.

The theory, while can be seen as a variant of the peridynamics (PD), has certain advantages over the PD, particularly when there is a loss of symmetry. The proposed directionality term avoids issues with correspondences under nonsymmetric conditions. We have performed buckling analysis of corrugated beam and found that the derivative-free formulation can provide accurate estimate the critical buckling load, while the derivative-based theories like the classical Timoshenko beam and couple-stress theory give erroneous estimates for the critical buckling load. The efficacy of the formalism has been showcased by solving multiple problems for different loading and boundary conditions. To bolster our claim, shear deformable beams with different core shapes are examined under three-point loading conditions and the results are validated against the well-established theories like couple-stress theory and sandwich theory. The results are found to be in good agreement with those obtained via 3-D FE models.

The authors would like to extend the study in the future to derive the nonlocal integro-differential models for other structural components such as plates and shells, considering the respective nonaffine energy expressions.

Acknowledgements The authors acknowledge Prof. Arun Srinivasa (Professor, Department of Mechanical Engineering, Texas A& M University, College Station, TX 77845, USA) for sharing his valuable comments and suggestions, which greatly improved the quality of the work. MS and SS acknowledge SERB (ECR/2018/001672) for supporting this work. The third author (JNR) acknowledges the support from the National Science Foundation (CMMI G. no. 1952873).

Author contributions All authors listed have made a substantial, direct and intellectual contribution to the work and approved it for publication.

Funding This study was partly supported by the Science and Engineering Research Board (SERB), India, under project ECR/2018/001672 to the first two authors. The third author was supported by a grant from the National Science Foundation (CMMI G. no. 1952873).

Declarations

Data availability The authors will make the data available on reasonable request.

Code availability All the codes will be shared on request.

Conflict of interest The authors declare that there are no competing interests with publication of this work.

Consent to participate All the authors give consent of participation in this manuscript.

Consent for publication All the authors give consent for publication of this manuscript.

Appendix A localization of derivative-free deformation gradient G

Here, we demonstrate that the derivative-free nonlocal directionality term approaches the classical deformation gradient in the infinitesimal limit. Let us assume sufficient smoothness of the field such that the displacement at a material point Y, in the neighbourhood of X, can be approximated using a truncated Taylor expansion as:

$$u(Y) \approx u(X) + \nabla(u, X)(Y - X), \tag{A1}$$

where ∇ is the classical gradient operator. The average stretch around X may also be approximated in a similar way.

$$\bar{u}(Y) \approx u(X) + \nabla(u, X)(\overline{Y - X}). \tag{A2}$$

The nonlocal derivative-free deformation gradient is expressed as:

$$\begin{aligned} G(u, X) &= I + \hat{G}(u, X) \\ &= I + \left[\int_{\Omega_x} (u - \bar{u}) \left(Y - \bar{Y}\right)^T dY\right] \left[\int_{\Omega_x} \left(Y - \bar{Y}\right) \left(Y - \bar{Y}\right)^T dY\right]^{-1}, \end{aligned} \tag{A3}$$

where I is the identity tensor. Replacing the terms in Eq. (A3) with those given in Eqs. (A1) and (A2), we get,

$$\begin{aligned} G &\approx I + \left[\int_{\Omega_x} \left(u(X) + \nabla(u, X)(Y - X) - (u(X) + \nabla(u, X)(\overline{Y - X}))\right) \left(Y - \bar{Y}\right)^T dY\right]. \\ &\quad I + \left[\int_{\Omega_X} (Y - \bar{Y})(Y - \bar{Y})^T dY\right]^{-1} \\ &= I + \left[\int_{\Omega_x} \nabla(u, X)(Y - X - \overline{Y - X}) \left(Y - \bar{Y}\right)^T dY\right] \left[\int_{\Omega_X} (Y - \bar{Y})(Y - \bar{Y})^T dY\right]^{-1} \\ &= I + \nabla(u, X) \left[\int_{\Omega_x} (Y - X - \bar{Y} - \bar{X}) \left(Y - \bar{Y}\right)^T dY\right] \left[\int_{\Omega_X} (Y - \bar{Y})(Y - \bar{Y})^T dY\right]^{-1} \\ &= I + \nabla(u, X) \left[\int_{\Omega_x} (Y - \bar{Y}) \left(Y - \bar{Y}\right)^T dY\right] \left[\int_{\Omega_X} (Y - \bar{Y})(Y - \bar{Y})^T dY\right]^{-1} \\ &= I + \nabla(u, X) \\ &= F. \end{aligned} \tag{A4}$$

References

1. Shan, S., Kang, S.H., Raney, J.R., Wang, P., Fang, L., Candido, F., Lewis, J.A., Bertoldi, K.: Multistable architected materials for trapping elastic strain energy. Adv. Mater. **27**, 4296–4301 (2015)
2. Liu, S., Azad, A.I., Burgueño, R.: Architected materials for tailorable shear behavior with energy dissipation. Extrem Mech. Lett. **28**, 1–7 (2019)

3. Reddy, J.N.: Personal Reflections of My Research in Structural Mechanics: Past, Present, and Future. In: EASEC 16, pp. 33-42. Springer (2021)
4. Kahrobaiyan, M.H., Asghari, M.: Ahmadian, M.T.3306644: A strain gradient Timoshenko beam element: application to MEMS. Acta Mech. **226**, 505–525 (2015)
5. Romanoff, J., Karttunen, A.T., Varsta, P., Remes, H., Reinaldo Goncalves, B.: A review on non-classical continuum mechanics with applications in marine engineering. Mech. Adv. Mater. Struct. **27**, 1065–1075 (2020)
6. Srinivasa, A.R., Reddy, J.N.: An overview of theories of continuum mechanics with nonlocal elastic response and a general framework for conservative and dissipative systems. Appl. Mech. Rev. **69**, 030802 (2017)
7. Cosserat, E., Cosserat, F.: Theorie des corps dédormables. (1992)
8. Eringen, A.C.: Nonlocal continuum field theories. Appl. Mech. Rev. **56**(2), 20–22 (1992)
9. Reddy, J.N.: Nonlocal theories for bending, buckling and vibration of beams. Int J Eng. Sci. **45**, 288–307 (2007)
10. Lim, C.W., Zhang, G., Reddy, J.N.: A higher-order nonlocal elasticity and strain gradient theory and its applications in wave propagation. J. Mech. Phys. Sol. **78**, 298–313 (2015)
11. Yang, F.A.C.M., Chong, A.C.M., Lam, D.C.C., Tong, Pin: Couple stress based strain gradient theory for elasticity. Int. J. Sol. Struct. **39**, 2731–2743 (2002)
12. Ma, H.M., Gao, X.-L., Reddy, J.N.: A microstructure-dependent Timoshenko beam model based on a modified couple stress theory. J. Mech. Phys. Sol. **56**, 3379–3391 (2008)
13. Reddy, J.N.: Microstructure-dependent couple stress theories of functionally graded beams. J. Mech. Phys. Sol. **59**, 2382–2399 (2011)
14. Gao, X.-L.: A new Timoshenko beam model incorporating microstructure and surface energy effects. Acta Mech. **226**, 457–474 (2015)
15. Silling, S.A.: Reformulation of elasticity theory for discontinuities and long-range forces. J. Mech. Phys. Sol. **48**, 175–209 (2000)
16. Silling, S.A., Epton, M., Weckner, O.: Xu, Ji, Askari, E23481501120: Peridynamic states and constitutive modeling. J. Elast. **88**, 151–184 (2007)
17. Gerstle, W., Sau, N., Silling, S.: Peridynamic modeling of concrete structures. Nuclear Eng. Design. **237**, 1250–1258 (2007)
18. Zhang, H., Li, Hui, Ye, H., Zheng, Y., Zhang, Y.: A coupling extended multiscale finite element and peridynamic method for modeling of crack propagation in solids. Acta Mech. **230**, 3667–3692 (2019)
19. Yu, H., Chen, X., Sun, Y.: A generalized bond-based peridynamic model for quasi-brittle materials enriched with bond tension-rotation-shear coupling effects. Comput. Methods Appl. Mech. Eng. **372**, 113405 (2020)
20. Wang, Y., Han, F., Lubineau, G.: Strength-induced peridynamic modeling and simulation of fractures in brittle materials. Comput. Methods Appl. Mech. Eng. **374**, 113558 (2021)
21. Wan, J., Chen, Z., Chu, X., Liu, H.: Improved method for zero-energy mode suppression in peridynamic correspondence model. Acta Mech. Sin. **35**, 1021–1032 (2019)
22. Aghababaei, R., Reddy, J.N.: Nonlocal third-order shear deformation plate theory with application to bending and vibration of plates. J. Sound Vibration. **326**, 277–289 (2009)
23. Lu, P., Zhang, P.Q., Lee, H.P., Wang, C.M., Reddy, J.N.: Non-local elastic plate theories. Proc. R. Soc. A Math. Phys. Eng. Sci. **463**, 3225–3240 (2007)
24. Srividhya, S., Raghu, P., Rajagopal, A., Reddy, J.N.: Nonlocal nonlinear analysis of functionally graded plates using third-order shear deformation theory. Int. J. Eng. Sci. **125**, 1–22 (2018)
25. Sarkar, S., Roy, D., Vasu, R.M.: A global optimization paradigm based on change of measures. R. Soc. Open Sci. **2**, 150123 (2015)
26. Sarkar, S., Roy, D., Vasu, R.M.: A Kushner-Stratonovich Monte Carlo filter applied to nonlinear dynamical system identification. Phys. D Nonlinear Phenom. **270**, 46–59 (2014)
27. Saxena, M., Sarkar, S., Roy, D.: A microstructure-sensitive and derivative-free continuum model for composite materials: Applications to concrete. Int. J. Sol. Struct. **262**, 112051 (2023)
28. Nowruzpour, M., Sarkar, S., Reddy, J.N., Roy, D.: A derivative-free upscaled theory for analysis of defects. J. Mech. Phys. Sol. **125**, 1–22 (2018)
29. de Sciarra, Francesco M., Barretta, R.: A gradient model for Timoshenko nanobeams. Phys. E Low Dimens. Syst. Nanostructures. **62**, 1–9 (2014)
30. Reddy, J.N.: Energy Principles and Variational Methods in Applied Mechanics. John Wiley & Sons, Hoboken (2017)
31. Goncalves, B.R., Karttunen, A.T., Romanoff, J.: A gradient model for Timoshenko nanobeams. Compos. Struct. **212**, 586–597 (2019)
32. Ban, H., Shi, G., Shi, Yongjiu, Bradford, M.A.: Experimental investigation of the overall buckling behaviour of 960 MPa high strength steel columns. J. Constr. Steel Res. **88**, 256–266 (2013)